Clays and Clay Minerals, Vol. 69, No. 6:759–771, 2021

DISPERSION AND SWELLABILITY OF TERNARY SURFACTANT CO-MODIFIED MONTMORILLONITES

Wei Hua Yu[1,2], Jia Hui Liu[2], Min Wang[2], Na Li[3], Jun Rui Zhang[1], Tian Hao Huang[1], and Chun Hui Zhou[2,4,5]*

[1]Zhijiang College, Zhejiang University of Technology, Shaoxing 312030, China
[2]Research Group for Advanced Materials & Sustainable Catalysis (AMSC), Breeding Base of State Key Laboratory of Green Chemistry Synthesis Technology, College of Chemical Engineering, Zhejiang University of Technology, Hangzhou 310032, China
[3]Tiantong Ruihong Technology Co., Ltd, Haining 314400, China
[4]Engineering Research Center of Non-metallic Minerals of Zhejiang Province, Zhejiang Institute of Geology and Mineral Resource, Hangzhou 310007, China
[5]Qing Yang Institute for Industrial Minerals, You Hua, Qing Yang 242804 An Hui, China

Abstract—Organo-montmorillonite (OMnt) has wide applications in paints, clay-polymer nanocomposites, biomaterials, etc. In most cases, the dispersibility and swellability of OMnt dictate the performance of OMnt in the target products. Previous studies have revealed that the properties can be improved when multiple organic species are co-introduced into the interlayer space of montmorillonite (Mnt). In the present study, single surfactant erucylamide (EA), dual-surfactants cetyltrimethyl ammonium bromide (CTAB) and octadecyltrimethyl ammonium chloride (OTAC), and ternary-surfactants EA, CTAB, and OTAC were co-introduced into Mnt by solution intercalation. The resulting OMnts were characterized by powder X-ray diffraction (XRD), Fourier-transform infrared (FTIR) spectroscopy, thermogravimetry-differential thermogravimetry (TG-DTG), water contact-angle tests, scanning electronic microscopy (SEM), laser particle-size analysis, and swelling indices. Mnt co-modified by ternary CTAB, OTAC, and EA led to a large d_{001} value (4.20 nm), surface hydrophobicity with a contact angle of 95.6°, swellability (50 mL/g) with small average particle sizes (2.1−2.8 μm) in xylene, and >99% of the OMnt particles were kept as <5 μm in deionized water. The formation of EA-modified-Mnt was proposed according to hydrophobic affinity, hydrogen bonding, and van der Waals forces. The nanoplatelets of the CTA^+, OTA^+, and EA co-modified OMnts in xylene were assembled into a house-of-cards structure by face-to-edge and edge-to-edge associations. The electrostatic attractions, electrostatic and steric repulsions, and hydrophobic interactions were responsible for the good dispersibility of OMnt in xylene. The ternary surfactant co-modified OMnt with high dispersion and swellability will make OMnt better suited for real-world applications.

Keywords—Co-modification · Dispersion · Hydrophobicity · Organo-montmorillonite · Ternary surfactants · Swellability

INTRODUCTION

Montmorillonite (Mnt), a natural aluminosilicate, is a layered clay mineral with platelet morphology (Ho & Glinka, 2003). Each platelet is composed of two sheets of silicon-oxygen in tetrahedral geometry sandwiching a central sheet of aluminum-oxygen in octahedral geometry (de Jong et al., 2014; Teich-McGoldrick et al., 2015). The isomorphic substitutions of some Al(III) ions in the octahedral sheet by Mg(II) or Fe(II), etc. and some Si(IV) ions in the tetrahedral sheet by Al(III) lead to negatively charged platelets (Madejová, 2003). To counterbalance these negative charges on the surfaces of Mnt platelets, some hydrated metal cations such as Ca^{2+}, Na^+, etc. are adsorbed in the interlayer spaces of Mnt (Salles et al., 2007). The generally high hydrophilicity of raw Mnt limits its application in organic environments. The hydrated metal cations in the interlayer spaces of Mnt can be exchanged by organic cations. Thus, hydrophilic inorganic Mnt becomes hydrophobic organo-montmorillonite (OMnt). The organic modification of Mnt has expanded its applications into many disciplines and technologies, including rheological control agents, clay polymer nanocomposites, leakage-resistant agents, cosmetics, coatings, lubricants, and oil-based drilling fluids, etc. (Burgentzlé et al., 2004; Leach et al., 2005; Zhuang et al., 2015).

The dispersibility and swellability of OMnt in solvents need to be taken into consideration for industrial applications. For polymer-OMnt nanocomposites, uniform dispersion of individual OMnt platelets (~1 nm thick) or a few OMnt platelets at the nanometer scale can improve mechanical, fire-retardancy, and gas-barrier properties (Burgentzlé et al., 2004). The long alkyl chains of surfactants could help to stabilize the suspension of OMnt particles (Patel et al., 2007). Cetyltrimethyl ammonium bromide (CTAB) and octadecyltrimethyl ammonium chloride (OTAC) are used commonly as the organic modifiers to prepare OMnt in industrial applications. It is difficult for a complete 1 CEC (cation exchange capacity of Mnt) of cetyltrimethylammonium (CTA^+) or octadecyl trimethyl ammonium (OTA^+) cations to be intercalated into the interlayer spaces of Mnt through ion exchange (He et al., 2010; Lapides et al., 2011). Besides, the OTAC or CTAB-modified OMnts exhibited a low swellability and non-uniform dispersion in the organic medium because the trimethyl ammonium cation is a hydrophilic group (Moraru, 2001; Zhuang et al., 2015; Yu et al., 2017). According to Moraru (2001), the swellability of OMnts depends mainly on the nature of the exchanged ions and strong bridging between

* E-mail address of corresponding author: clay@zjut.edu.cn
DOI: 10.1007/s42860-021-00149-2

the platelets of the alkylammonium-modified OMnts due to the existence of electrostatic attraction. Their platelets, therefore, cannot be exfoliated fully.

Erucylamide (EA), a non-ionic surfactant, is one of the most important derivatives of erucic acid. Its super-long carbon-chain structure gives it excellent surface properties (Sankhe et al., 2003; Shuler et al., 2004). In addition, it is non-toxic(Hamberger & Stenhagen, 2003), used extensively as a slip or release agent in the polymer processing industry (Sankhe & Hirt, 2002; Poisson et al., 2010; Moreira et al., 2016), and as a variety of functional additives in printing inks, anti-binders, lubricants, plasticizers, plastic products for food packaging, coatings, etc. CTAB, OTAC, and EA have different polarities and hydrophobicity. CTAB has shorter alkyl chain than OTAC and EA. The co-modification of OTAC and EA onto Mnt led to a high swell index (100%) in xylene and tailored surface hydrophobicity of OMnts (Zhou et al., 2019). The OTAC and EA co-modified OMnts were aggregated into large particles (≥5 μm) in xylene. Both OTAC (clogP = 8.688) and EA (clogP = 8.408) have similar hydrophobicity and similar alkyl chain lengths, which brought about inflexible hydrocarbon chains in the interlayer spaces of Mnt and prevented more surfactants from entering the interlayer spaces. Co-modification of Mnt with CTAB, OTAC, and EA can make the arrangement of the long alkyl chains flexible and adsorb more surfactants into the interlayer spaces. Furthermore, co-introduction of ternary surfactants onto Mnt can improve surface properties of Mnt and increase the d_{001} value. For example, Liao et al. (2016) found that co-modification of ternary-surfactant CTAB, sodium dodecyl sulfate (SDS, anionic surfactant), and hydrogenated castor oil (nonionic surfactant) onto Na^+-Mnt led to a large d_{001} value (4.14 nm) and a large contact angle (90°). Co-adsorption of ternary-surfactant CTAB, SDS, and lauryl alcohol ethoxylated (nonionic surfactant) onto calcium bentonite resulted in a swelling index in mineral oil or isopropanol (6–10 mL/g), a high d_{001} value (~4.42 nm), and a contact angle of 79.76° (Monteiro et al., 2018). So far, however, to the best of the present authors' knowledge, no study on the co-modification of ternary-surfactant CTAB, OTAC, and EA onto Mnt has been reported.

The present study aimed to determine the effects of non-ionic EA on the microstructure, dispersion, and swellability of OMnts. A further purpose was to understand the interaction mechanisms between EA molecules and Mnt. The overarching goal was to provide novel information in the development of new OMnts with finer particle sizes, stable dispersion, and high swellability toward industrial applications.

EXPERIMENTAL

Materials

Ca^{2+}-Mnt was obtained from Anji, Zhejiang, China. Its CEC is 69.5 meq/100 g which was measured by the ammonium chloride-HCHO titration method (Zhu et al., 2008; Yu et al., 2014). Its chemical formula is $(Ca_{0.34}Na_{0.02}K_{0.14})[Al_{2.83}Fe(III)_{0.17}Mg_{1.23}][Si_{7.93}]O_{20}(OH)_4$. CTAB ($C_{16}H_{33}N(CH_3)_3Br$, analytical grade, ≥99.0%) was procured from Shanghai Baiao Bioscience and Technology Co., Ltd. (Shanghai, China). EA (*cis*-$C_8H_{17}CH{=}CH(CH_2)_{11}CONH_2$, analytical grade, ≥85.0%) was obtained from Shanghai Aladdin Biochemical Technology Co., Ltd. (Shanghai, China). OTAC ($C_{18}H_{37}N(CH_3)_3Cl$, analytical grade, ≥99.0%) and $AgNO_3$ (analytical grade, ≥99.8%) were purchased from Sinopharm Chemical Reagent Co., Ltd. (Shanghai, China). Ethylene glycol (analytical grade, ≥95.0%) and xylene (analytical grade, ≥99.0%) were purchased from Hangzhou Shuanglin Chemical Reagents Co., Ltd. (Hangzhou, China). Na_2CO_3 (analytical grade, ≥99.8%) was purchased from Taicang Meida Reagent Co., Ltd. (Taicang, Jiangsu, China).

Characterization

Powder X-ray diffraction (XRD) patterns were recorded on a PANalytical X'Pert PRO X-ray diffractometer (PANalytical, Almelo, The Netherlands) using Cu Kα radiation (λ = 1.542 Å). Fourier-transform infrared (FTIR) spectra were recorded using a Nicolet 6700 FTIR spectrometer (Thermo-Nicolet, Madison, Wisconsin, USA) and the KBr-sample pellet method. Thermogravimetry-differential thermogravimetry (TG-DTG) analyses were carried out on Mettler Toledo TGA/DSC 1 instrument (Mettler Toledo Corp., Zurich, Switzerland) at a temperature ramp of 10°C/min from room temperature to 800°C in N_2 atmosphere.

Water contact angles of the samples were measured using a Krüss-DSA100 goniometer (Hamburg, Germany) by the sessile drop method. Surface morphologies of the samples were observed under a Hitachi S-4700 (Hitachi, Ibaraki, Japan) scanning electron microscope (SEM). In each experiment, a very small amount of the powder sample was placed on a stub and then coated with gold prior to recording the images. The acceleration voltage was set at 2–10 kV.

Particle-size distributions of the dry powder samples dispersed in deionized water were measured using a Winner 2005A Laser Particle Size Analyzer (Jinan, Shandong, China). The instrument provided a continuous volume percentage of particle sizes in a range of 0.01–200 μm. Before measurement, 2 wt.% of the dry powder was dispersed in deionized water by using sonication to ensure the uniform dispersion of particles. Average particle sizes of the OMnt samples dispersed in xylene were tested using a Zetasizer nano ZS90 (Malvern Instruments Ltd., Worcestershire, UK). 0.2 g of dry OMnt particle powder was added to xylene (10 mL) and stirred for 30 min. After sonicating for a further 20 min, the resulting suspension of OMnt in xylene was measured five times to obtain the average particle sizes.

Swelling indices of the OMnt samples were measured in xylene. 1 g of OMnt was added to xylene (50 mL) and then stirred for 30 min at room temperature to obtain the mixture. After leaving the mixture static for 1–96 h, swelling indices (mL/g) were determined according to the volume of OMnt swollen in xylene.

Preparation of OMnt

Na-modification and purification of Mnt. 5 g of raw Ca^{2+}-Mnt powder was dried at 105°C for 12 h. Then, the dried Ca^{2+}-Mnt was dispersed uniformly in a solution of Na_2CO_3

https://doi.org/10.1007/s42860-021-00149-2 Published online by Cambridge University Press

(0.25 g in 75 mL of deionized water) to transform it into Na^+-Mnt by ion-exchange. The resulting mixture was stirred for 1 h at room temperature, and then kept at 60°C for 3 h. The mixture was kept static for a week at room temperature, then purified, first by gravity sedimentation followed by centrifugation at 5000×*g* for ~2 min using a TDL-5-A Flying Pigeon centrifuge (Shanghai Anting Scientific Instrument Factory, Shanghai, China). The distances from the sediment and suspension surfaces to the axis of the centrifuge rotor were 12.8 and 6.0 cm, respectively. According to Stokes' law, the size of purified Mnt particles was estimated to be ~4 μm (Veiskarami et al., 2016). The supernatant with dispersed particles (~≤4 μm in diameter) was collected and identified as purified Na^+-Mnt suspension for the next organic modification.

Surfactant modification of Mnt. Typically, 0.50 CEC of CTAB, 1.0 CEC of OTAC, and a certain amount of EA were dispersed in 25 mL of ethylene glycol. The surfactant mixture was kept at 80°C for 1 h with vigorous stirring and then the purified Na^+-Mnt suspension was added dropwise. The resulting mixture of the surfactants and Na^+-Mnt suspension was stirred vigorously at 80°C for 3 h to obtain the OMnt suspension, which was then cooled to room temperature, centrifuged, and washed with deionized water to remove the excess surfactants until no halide ions were detected. The OMnt was air dried at 80°C for 12 h and ground into a fine powder and sieved with a 200-mesh sieve. The OMnt samples were labeled as COE(*x*)/Mnt, where C, O, and E refer to CTAB, OTAC, and EA, respectively; *x* was the fraction (0.25, 0.50, 0.75, or 1.0) of the CEC of Ca^{2+}-Mnt of EA that was added. CO/Mnt and E(1.5)/Mnt were prepared in a similar way to COE(*x*)/Mnt. In the preparation of E(1.5)/Mnt, 1.5 CEC of EA was added to the Na^+-Mnt suspension without adding CTAB and OTAC, whereas in the preparation of CO/Mnt, no EA was added and the amount of CTAB and OTAC added was the same as for COE(*x*)/Mnt.

RESULTS AND DISCUSSION

XRD Patterns

The XRD patterns of Na^+-Mnt and OMnts (Fig. 1) revealed that the reflection of E(1.5)/Mnt at 5.96°2θ was the same as pure EA and Na^+-Mnt, demonstrating that pure EA solid has a molecular crystal structure. According to the Bragg equation, the d_{001} value for both Na^+-Mnt and E(1.5)/Mnt was 1.48 nm, indicating that EA adsorption caused no layer expansion and, thus, leading to the conclusion that EA molecules did not enter the interlayer spaces of Na^+-Mnt by cation exchange. This would not be surprising because the EA molecule is a non-ionic surfactant.

CO/Mnt exhibited a (001) reflection at 4.38°2θ (2.02 nm). Hence, the co-modification of Na^+-Mnt with dual surfactants of CTAB and OTAC led to an expansion of the interlayer space from 1.48 nm to 2.02 nm by ion exchange. Others (e.g. Xi et al., 2004; Yu et al., 2014) have shown that CTAB and/or OTAC can be arranged in various configurations in the interlayer of OMnt (Fig. 2), including as a lateral monolayer, lateral bilayer, pseudotrilayer, paraffin-type monolayer, and paraffin-type bilayer, giving d_{001} values of 1.45−1.47, 1.75−1.85, 1.91−2.02, 2.25−2.50, and 3.85−4.14 nm, respectively. Thus, with a d_{001} of 2.02 nm (Fig. 1) the CTA^+ and OTA^+ cations adopted a pseudotrilayer model in the interlayer spaces of CO/Mnt.

COE(0.25)/Mnt exhibited the same (001) reflection at 4.38°2θ as CO/Mnt (Fig. 1). The result indicated that the small amount of EA added (0.25 CEC) in the preparation of OMnt had little impact on the intercalation of the CTAB, OTAC, and EA surfactants into the interlayer spaces of Na^+-Mnt. COE(*x*)/Mnt (x = 0.50−1.0) exhibited the dual reflections at 2.11°2θ (d_{001} = 4.20 nm) and 4.38°2θ (d_{001} = 2.02 nm). This result suggested that the CTAB, OTAC, and EA surfactants were arranged heterogeneously in the interlayer spaces, in a paraffin-type bilayer and pseudotrilayer in COE(*x*)/Mnt (x = 0.50−1.0) (Fig. 2). The heterogeneous introduction of surfactants to the interlayer space is commonly found in organic modifications of Mnt (Xi et al., 2005; Kooli et al., 2009; Yu et al., 2014). The increase in the d_{001} value indicated that adding large amounts of EA (i.e. >0.25 CEC) may also have facilitated the entry of EA molecules into the interlayer spaces of Mnt.

Based on the XRD patterns described above (Fig. 1), the OTA^+ and CTA^+ cations first entered the interlayer spaces of Mnt by ion exchange, and then EA molecules were drawn into the interlayer spaces by the alkyl chains of the OTA^+ and CTA^+ cations, the driving force being the hydrophobic affinity between the alkyl chains of the surfactants.

FTIR Spectra

All the OMnts retained the characteristic Si–O–Si, Si–O–Al, and structural hydroxyl bands from Mnt (Table 1). For COE(*x*)/Mnt, the 3429 cm^{-1} band from interlayer water seen in the spectrum for Na^+-Mnt disappeared (Fig. 3), demonstrating the diminishing amount of water in the interlayer spaces of OMnt due to introduction of the organic surfactants (Parolo et al., 2014), as confirmed by the mass losses below 120°C (2.2–2.8% for COE(*x*)/Mnt and 8.9% for Na^+-Mnt, Table 2). The 1469, 2850, and 2921 cm^{-1} (C–H) bands for all the OMnts were detected because of the adsorption of the alkyl chains of the surfactants on Mnt. The Si-O band at 1039 cm^{-1} observed in sample Na^+-Mnt was unchanged in sample E(1.5)/Mnt, whereas in samples CO/Mnt and COE(*x*)/Mnt, it was split into two distinct bands, at 1039 cm^{-1} (in-plane Si–O stretch) and 1097 cm^{-1} (out-of-plane Si–O stretch) (Madejová & Komadel, 2001; Zatta et al., 2013). The strong electrostatic interactions between the polar OTA^+ and CTA^+ cations in the interlayer spaces of Mnt and the polar negatively charged Si–O groups in the tetrahedral sheet of Mnt changed the Si–O vibration modes, but this splitting was absent from the spectrum of E(1.5)/Mnt because the polarity of non-ionic EA is lower than that of OTA^+ and CTA^+ cations.

The amide I band from C=O stretching at 1645 cm^{-1} is characteristic of the pure EA crystal (Fig. 3), indicating a strong interaction among the EA molecules through hydrogen

https://doi.org/10.1007/s42860-021-00149-2 Published online by Cambridge University Press

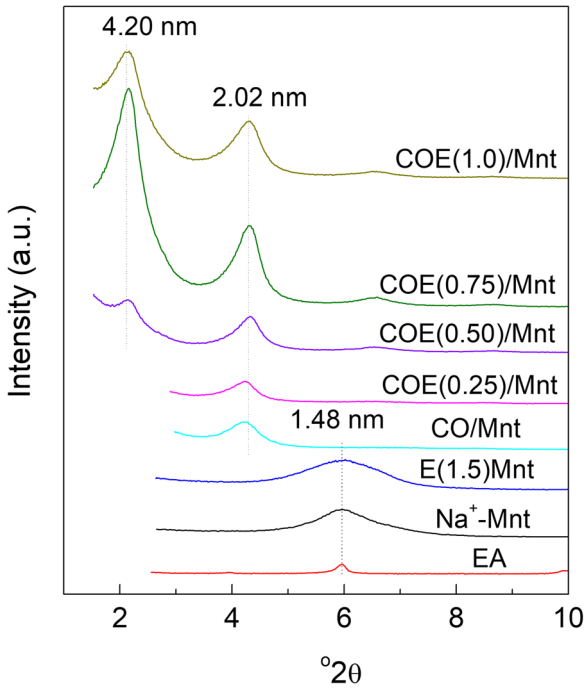

Fig. 1. Powder XRD patterns of Na^+-Mnt, EA, and OMnts

bonding. Other bands observed in the pure EA were derived from N–H (3191 and 3361 cm^{-1}) and C–N (1423 cm^{-1}). Sample E(1.5)/Mnt exhibited these same absorption bands, unperturbed by the Mnt, thus providing strong evidence that the EA molecules were adsorbed to the external surfaces. The coverage of external surfaces by the solid-like EA molecules apparently was extensive, as indicated by the mass loss of 41.5 wt.% in the 120–520°C region of the TG-DTG curves (see below, Fig. 5, Table 2). This finding was in accordance with the XRD patterns above.

All the COE(*x*)/Mnt samples exhibited the amide I C=O bands at 1666–1670 cm^{-1} due to adsorption of EA. Their amide I C=O bands shifted from 1645 cm^{-1} to higher wavenumbers 1666–1670 cm^{-1} compared with those of pure EA and E(1.5)/Mnt. Co-modification of CTAB, OTAC, and EA onto Mnt broke the large association via hydrogen bonds among EA molecules adsorbed on the external surfaces. A 20 wt.% EA/quaternaryammonium-modified OMnt was prepared by Ratnayake et al. (2009) by melt mixing at 100°C; those authors found that the amide I band shifted from 1645 cm^{-1} for pure EA to a higher wavenumber (1670 cm^{-1}) after adsorption of EA onto the quaternary ammonium-modified OMnt. A similar finding was reported by Moreira et al. (2016). In addition, COE(*x*)/Mnt also exhibited a shift of the N–H bands from 3361 cm^{-1} towards higher wavenumbers (3388–3450 cm^{-1}) due to the breakage of hydrogen bonds between EA molecules adsorbed on Mnt. The results from Fig. 3 suggested, therefore, that the EA molecules adsorbed on COE(*x*)/Mnt were well dispersed at the molecular level (Ratnayake et al., 2009).

For COE(*x*)/Mnt, the intensity of the C=O and N–H bands increased with increasing amounts of EA added from 0.25 to

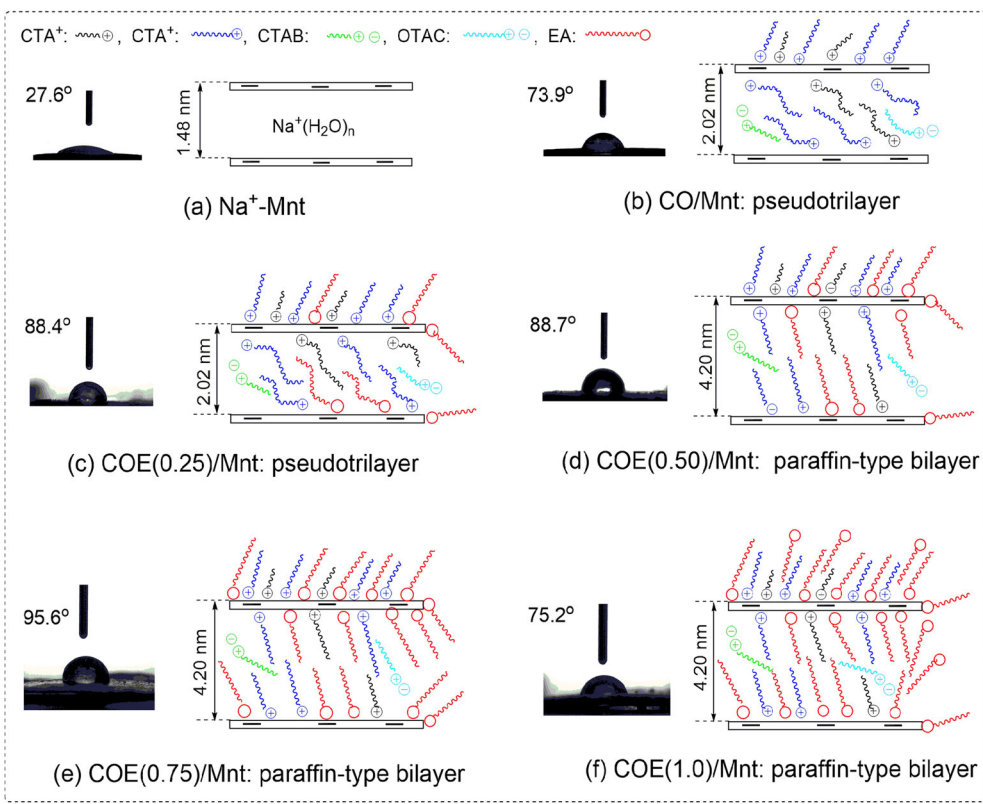

Fig. 2. Arrangement models of the surfactants adsorbed on OMnts and contact angles of Na^+-Mnt and OMnts

https://doi.org/10.1007/s42860-021-00149-2 Published online by Cambridge University Press

Table 1. Assignment of vibrational absorption bands in the FTIR spectra of Na^+-Mnt and OMnts

Wavenumber (cm^{-1})	Assignment	Ref.
476, 518	Bending vibrations of Si–O–Si and Si–O–Al (octahedral Al) groups in the the Mnt lattice, respectively.	(Madejová, 2003)
842, 908	Bending vibrations of Al(Mg)–OH and Al(Al)–OH hydroxyl groups in the octahedral sheet, respectively.	(Madejová, 2003)
1039, 1097	Stretching and out-of-plane bending vibrations of Si–O group in the tetrahedral sheet, respectively.	(Madejová & Komadel, 2001; Zatta et al., 2013)
1640	H–O–H bending vibration from adsorbed water	(Madejová & Komadel, 2001)
3429, 3616	Stretching vibrations of the interlayer water OH and structural hydroxyl groups (Al–OH) in the octahedral sheet, respectively.	(Madejová & Komadel, 2001; Shah et al., 2013)
1469, 2850, 2921	C–H scissoring, asymmetric and symmetric stretching vibrations from $–CH_2$, respectively.	(Li & Ishida 2003; Khenifi et al., 2007)
1645, 1666–1670	Stretching vibration of the amide I C=O in associative state (hydrogen bond) and in free dispersed state, respectively.	(Ratnayake et al., 2009; Moreira et al., 2016)
3191, 3361–3450	N–H symmetric and asymmetric stretching vibrations from $–CONH_2$, respectively.	(Zhou et al., 2019)
1423	C–N stretching vibration from $–CONH_2$	(Ghazy et al., 2020)

0.75 CEC, and then decreased when the amount of EA added increased further to 1.0 CEC. COE(0.75)/Mnt exhibited the strongest absorption peaks of the C=O and N–H bands, for two probable reasons: (1) COE(0.75)/Mnt had a large amount of EA loading (52.3 wt.% of mass loss in the 120–520°C region, Table 2); and (2) the arrangements of the surfactants (molecules and cations) were more ordered in the interlayer spaces of COE(0.75)/Mnt than in COE(x)/Mnt (x = 0.25, 0.50, and 1.0), as confirmed by the XRD patterns above.

Adsorption Mechanisms

Adsorption mechanisms of the surfactants (CTAB, OTAC, and EA) onto Mnt involve electrostatic attraction, hydrophobic interaction, hydrogen bond, and van der Waals forces (Fig. 4). Firstly, CTA^+ and OTA^+ cations were intercalated into the interlayer spaces of Mnt by cation exchange due to electrostatic interaction (Fig. 4a)(Xi et al., 2004). Then, the outer EA molecules, CTAB, and OTAC molecules in the form of ion pairs (CTA^+-Br^-

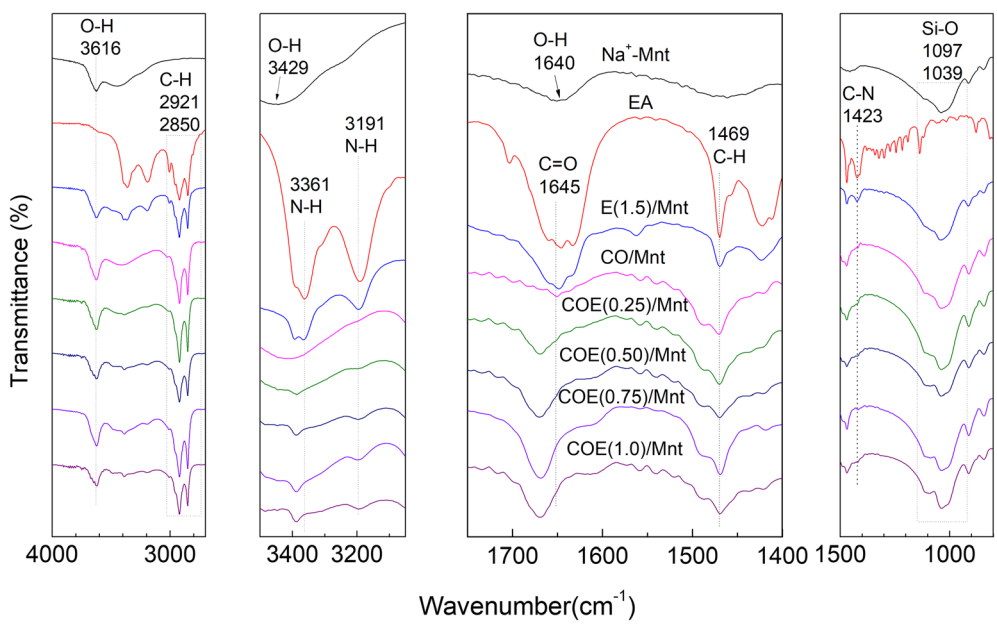

Fig. 3. FTIR spectra of Na^+-Mnt, EA, and OMnts

https://doi.org/10.1007/s42860-021-00149-2 Published online by Cambridge University Press

Table 2. Mass losses (%) in the different temperature stages from the TG data (compare with Fig. 5)

Sample	Dehydration (%) (<120°C)	Desurfactant (%)				Dehydroxylation (%) (520–750°C)
		120–300°C	300–360°C	360–520°C	120–520°C	
Na^+-Mnt	8.9	0.0	0.0	0.0	0.0	4.8
CTAB	0.0	99.0	0.5	0.2	99.7	–
OTAC	2.0	91.3	0.3	0.2	91.8	–
EA	0.0	20.8	75.8	1.5	98.1	–
CO/Mnt	3.2	24.4	6.7	10.0	41.1	2.4
E(1.5)/Mnt	5.0	16.7	17.8	7.0	41.5	3.4
COE(0.25)/Mnt	2.8	21.7	13.2	10.3	45.2	2.6
COE(0.50)/Mnt	2.3	19.9	18.5	8.3	46.7	2.0
COE(0.75)/Mnt	2.6	22.6	20.1	9.6	52.3	1.9
COE(1.0)/Mnt	2.2	22.1	23.5	9.1	54.7	2.2

and OTA^+-Cl^-) were drawn into the interlayer spaces of Mnt by the long alkyl chains of the CTA^+ and OTA^+ adsorbed in the interlayer spaces of Mnt in the first step due to strong hydrophobic affinity (Fig. 4b)(Meleshyn & Bunnenberg, 2006). Meanwhile, OTA^+ and CTA^+ could also be adsorbed onto the external exposed-face surfaces of Mnt by electrostatic attraction (Fig. 4c) between the CTA^+ and OTA^+ cations and the negatively charged platelets of Mnt (Xi et al., 2004). CTA^+ and OTA^+ cations were scarcely adsorbed at the positively charged edges of Mnt under neutral conditions due to their electrostatic repulsions (van Olphen, 1964; Patel et al., 2007).

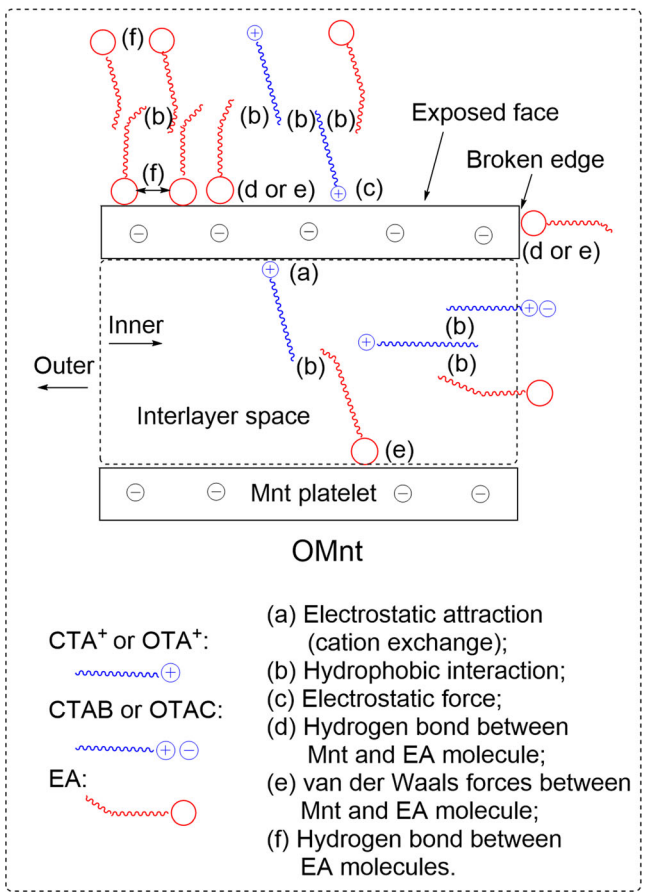

Fig. 4. Adsorption mechanisms of EA, CTAB, and OTAC onto Mnt

https://doi.org/10.1007/s42860-021-00149-2 Published online by Cambridge University Press

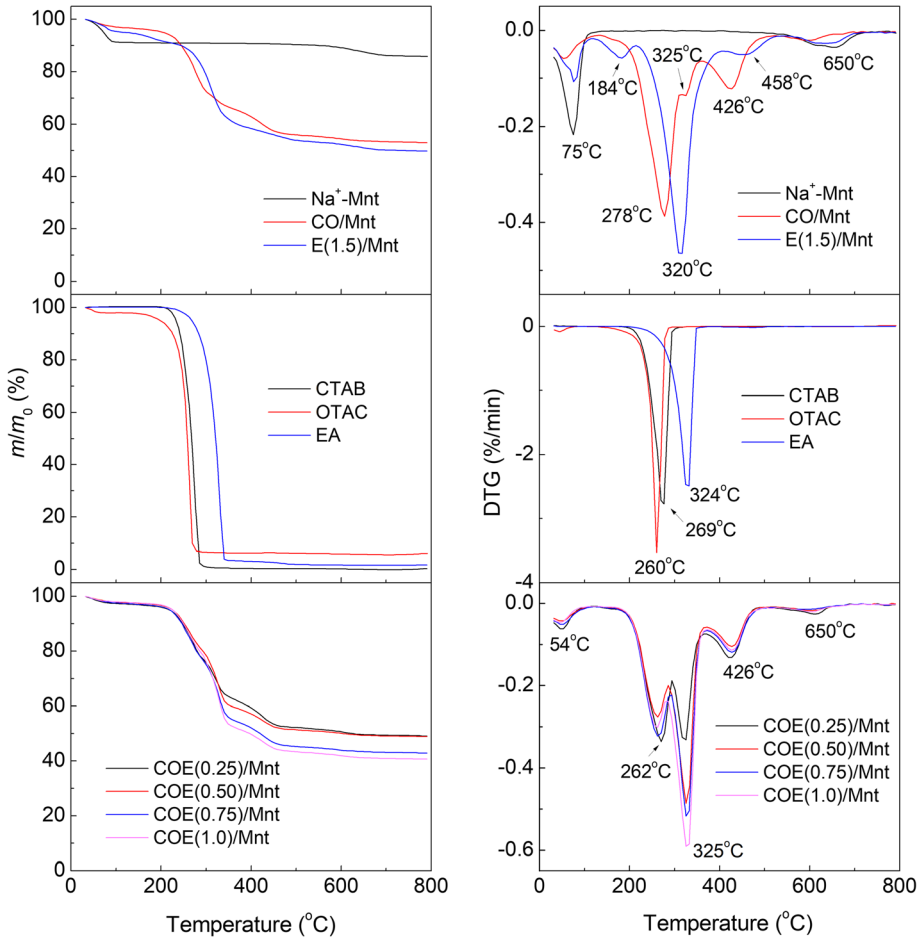

Fig. 5. TG-DTG curves of Na^+-Mnt, EA, CTAB, OTAC, and OMnts

For the adsorption of nonionic EA surfactant onto Mnt, besides hydrophobic affinity (Fig. 4b), hydrogen bond and van der Waals forces are also driving forces. Some silanol (Si–OH) groups are present on the exposed faces (Shattar et al., 2020) and at the broken edges of Mnt, some silanol (Si–OH) and aluminol (Al–OH) groups also exist (Burgentzlé et al., 2004). Hence, EA molecules can be bound to the exposed face and edge surfaces of Mnt through hydrogen bonds between the $CONH_2$ groups of EA molecules and the silanol (Si–OH) and aluminol (Al–OH) groups of Mnt (Fig. 4d). Certainly, the polar $CONH_2$ groups of EA molecules can also interact through van der Waals forces with the polar sites of the Mnt silicate layers on the inner and outer surfaces (Fig. 4e).

Hydrogen bonds between EA molecules adsorbed on the surfaces of Mnt (Fig. 4f) and hydrophobic interactions among the long alkyl chains of EA molecules and the surfactant cations (OTA^+ and CTA^+) (Fig. 4b) made the co-adsorption of the ternary surfactants onto Mnt more complex.

TG-DTG Analyses of OMnt

A TG test can be used to study the thermal stability of OMnt and packing arrangement of the intercalated surfactants in OMnt. The TG-DTG curves of the Na^+-Mnt, EA, CTAB, OTAC, and OMnts modified by single organic species (EA), dual organic species (CTAB and OTAC), and ternary organic species (EA, CTAB, and OTAC) are displayed in Fig. 5. The TG-DTG curves of Na^+-Mnt and all the OMnts showed the mass losses in the 50–120°C and 520–750°C regions due to the elimination of the physically adsorbed water and structural –OH groups of Mnt, respectively (Xi et al., 2007; Ikhtiyarova et al., 2012).

The pure CTAB, OTAC, and EA solids exhibited only one stage of mass loss in the 120−520°C region. The mass losses were 99.2, 91.1, and 96.7% for pure CTAB, OTAC, and EA solids in the 184−310, 140−294, and 200−364°C regions, which were close to their mass losses in the 120−520°C region, respectively (Table 2). The results suggested that the pure CTAB, OTAC, and EA solids were decomposed completely at 310, 294, and 364°C, respectively. EA exhibits the greatest thermal stability, whereas the thermal stability of pure CTAB and OTAC solids is less than EA but similar to each other.

The mass losses for CO/Mnt in the 120−300, 300−360, and 360−520°C regions corresponded to removal of the CTA^+ and OTA^+ cations adsorbed on the external surfaces of Mnt (24.4%), the CTAB and OTAC molecules bound in the interlayer spaces of Mnt (6.7%), and the CTA^+ and OTA^+ cations adsorbed in the interlayer spaces of Mnt (10.0%) (Xi et al.,

https://doi.org/10.1007/s42860-021-00149-2 Published online by Cambridge University Press

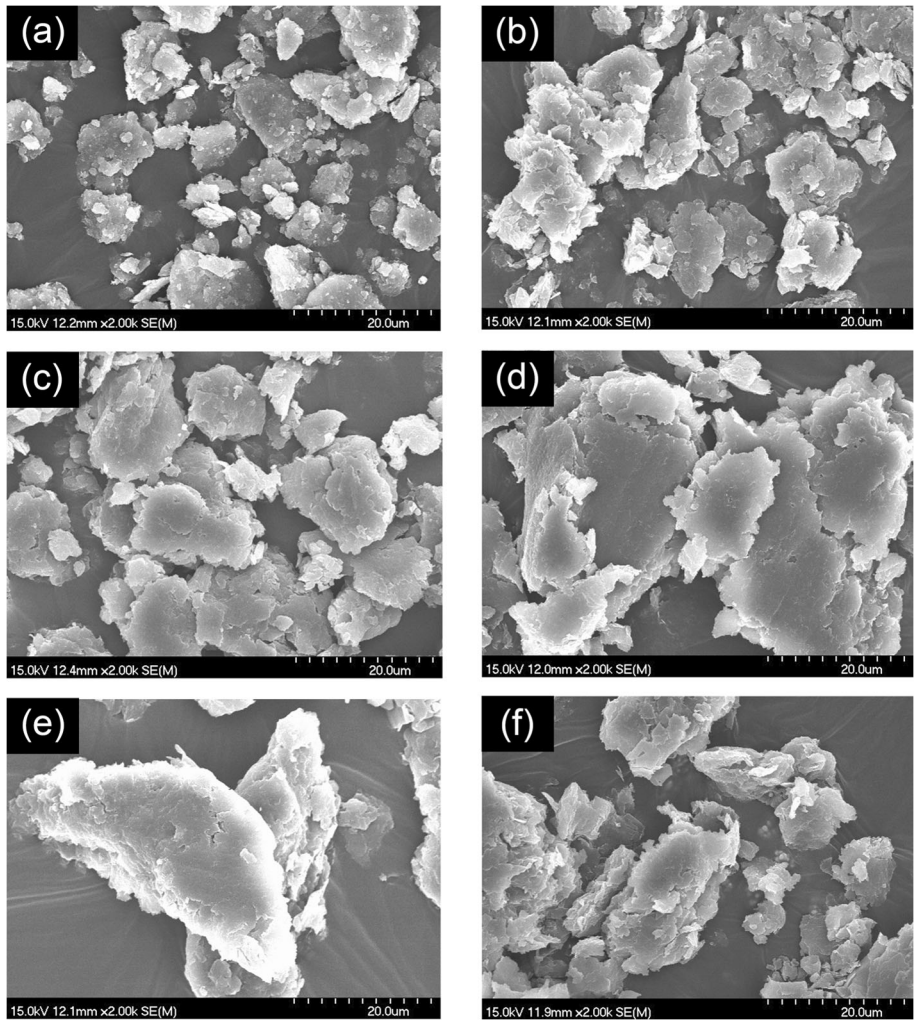

Fig. 6. SEM images of **a** Na^+-Mnt, **b** CO/Mnt, and **c** COE (*x*)/Mnt: *x* = 0.25, **d** 0.50, **e** 0.75, and **f** 1.0

2005), respectively. The decomposition temperatures for the CTAB and OTAC surfactants (molecules and cations) adsorbed on CO/Mnt were different from those for the pure CTAB and OTAC solids due to the different adsorption sites of Na^+-Mnt and the various interactions (Fig. 4) between the CTAB and OTAC surfactants (molecules and cations) and the Mnt silicate layers (Xi et al., 2005; Yu et al., 2014).

E(1.5)/Mnt displayed three stages of mass loss due to removal of adsorbed EA molecules, in the ranges of 120−215°C (3.7%), 215−419°C (33.8%), and 419−520°C (4.0%). The total mass loss was 41.5% in the 120−520°C region. Such thermal behavior was different from that for the pure EA solid, and indicated that the EA molecules adsorbed on E(1.5)/Mnt appeared in three different molecular environments. The mass loss in the 120−215°C region (3.7%) was attributed to the removal of the well dispersed EA molecules at the molecular level from the external surfaces of Mnt which were held by weak van der Waals forces (Fig. 4e). There are no hydrogen bonds between these EA molecules.

Table 3. Particle sizes of the samples dispersed in deionized water and in xylene

Sample	Particle size in deionized water			D^b (μm)
	$D_{50}{}^a$ (μm)	$D_{99}{}^a$ (μm)	<5 μm (%)	
Na^+-Mnt	0.9	3.9	99.7	-
CO/Mnt	1.0	7.6	98.1	3.8
E(1.5)/Mnt	0.8	4.9	99.1	-
COE(0.25)/Mnt	0.9	5.4	98.8	2.8
COE(0.50)/Mnt	0.8	2.7	99.9	2.4
COE(0.75)/Mnt	0.7	3.9	99.4	2.2
COE(1.0)/Mnt	0.7	3.9	99.5	2.1

[a] D_{50} and D_{99} refer to the particle sizes corresponding to the sample with cumulative volume percentages of 50% and 99%, respectively

[b] Average particle sizes of the OMnts in xylene

https://doi.org/10.1007/s42860-021-00149-2 Published online by Cambridge University Press

The mass-loss temperature range of the second stage (215–419°C) was close to that of the pure EA solid (200–364°C), suggesting that >80% of the mass loss over the 120–520°C region came from EA in a nearly pure phase mixed with the Mnt. This is consistent with the XRD data and the FTIR spectra that indicated these EA molecules were not introduced into the interlayer spaces but existed mainly in a solid-like state (namely a pseudo-pure phase of EA) on the external surface of Mnt. The extent of interaction between this phase and the Mnt is unclear besides van der Waals forces, but some interactions such as hydrogen bonds between these EA molecules (Fig. 4f) were probably present because the decomposition temperature was slightly greater than for the pure EA crystals.

The mass loss (4.0%) in the highest-temperature region (419–520°C) corresponded to the EA molecules being more tightly bound, for example, via hydrogen bonding between the $CONH_2$ groups of the EA molecules and the silanol (Si–OH) and aluminol (Al–OH) groups exposed at the edges and plane face surfaces of the Mnt (Fig. 4d)(Ratnayake et al., 2009).

Co-modification of the Mnt by CTAB, OTAC, and EA made the thermal behavior complex. As in EA(1.5)/Mnt, three stages of mass loss with increasing temperature were observed in COE(x)/Mnt, in the 120–300, 300–360, and 360–520°C regions. In light of the thermal decomposition behaviors of CO/Mnt and E(1.5)/Mnt, of the XRD patterns, and of the FTIR spectra above, the mass loss from COE(x)/Mnt in the 120–300°C region (first step) was probably due to the decomposition of the well dispersed EA molecules at the molecular level bound by van der Waals forces and of the CTA^+ and OTA^+ cations electrostatically adsorbed on the external surfaces of the Mnt.

The mass loss in the 300–360°C region (second step) corresponded to removal of the EA molecules in a solid-like state on the external surfaces of Mnt and by the interlayer OTAB and OTAC molecules, along with EA attracted to the OTAB and OTAC hydrophobic interlayer sites. The mass loss in the 360–520°C region (third step) was mainly caused by the elimination of the inner ion-exchanged OTA^+ and CTA^+ cations and the outer hydrogen bonded EA molecules.

The dehydration below 120°C for Na^+-Mnt, CO/Mnt, COE(x)/Mnt, and E(1.5)/Mnt was 8.9, 3.2, 2.2–2.8, and 5.0% respectively. Compared to Na^+-Mnt, all the OMnts contained less physically absorbed water due to adsorption of the hydrophobic organic surfactants. Moreover, CO/Mnt and COE(x)/Mnt contained less interlayer water compared with E(1.5)/Mnt because most of the hydrated cations (Na^+) in the interlayer spaces of Mnt were replaced by OTA^+ and CTA^+, whereas for E(1.5)/Mnt, no EA molecules entered the interlayer spaces, leaving only Na^+.

Mass losses of the surfactants adsorbed on E(1.5)/Mnt and CO/Mnt in the 120–520°C region were 41.1 and 41.5%, respectively. For COE(x)/Mnt, the amount of the adsorbed surfactants was equal to the mass loss in the 120–520°C region and increased from 45.2 to 54.7% as the addition of EA increased from 0.25 to 1.0 CEC.

Contact Angles

The surface and interface properties of OMnt are important for its use in organic systems. The solid-water contact angle reflects the surface hydrophobicity or hydrophilicity of a solid material (Alghunaim et al., 2016); the larger the contact angle of the material, the greater the surface hydrophobicity. Na^+-Mnt is hydrophilic and its contact angle was 27.6°. After introduction of CTA^+ and OTA^+ , the contact angle increased to 73.9° (for sample CO/Mnt) which is similar to the reported value (Liao et al., 2016).

The contact angles of COE(x)/Mnt (x = 0.25 and 0.50) were similar to each other (88.4° and 88.7°), but when x increased to 0.75 (COE(0.75)/Mnt), a maximum contact angle of 95.6° was reached. On the other hand, when x increased further to 1.0 (sample COE(1.0)/Mnt), the contact angle dropped to only 75.2°. The values of contact angle depend on the loading amounts of surfactants and the orientation of the hydrophobic groups on the outer surfaces (Zhuang et al., 2016). At low surfactant loadings of COE(x)/Mnt (x = 0.25, 0.50, and 0.75) (mass losses of 45.2–52.3% in the 120–520°C region, Table 2), the hydrophilic groups were close to the hydrophilic polar sites of the Mnt silicate layers, whereas the hydrophobic groups were pointed outward (Fig. 2c, d, e). For COE(1.0)/Mnt, when the hydrophilic polar sites of the Mnt silicate layers were occupied by the hydrophilic groups, some hydrophilic groups were oriented outward (Fig. 2f) due to a high surfactant loading (mass loss of 54.7% in the 120–520°C region, Table 2).

Morphology of OMnt

The particle sizes of COE(x)/Mnt were ~4–40 μm larger than those of Na^+-Mnt (~1–10 μm) and CO/Mnt (~2–10 μm) because of greater aggregation in COE(x)/Mnt. Most Na^+-Mnt particles existed in the form of aggregates of oblate (plate-like) particles ~1–10 μm, and all the OMnts also looked oblate (Fig. 6). The trend in particle size of COE(x)/Mnt followed its contact angle trend, with COE(0.75)/Mnt showing the most massively aggregated particles due to high surface hydrophobicity (high contact angle of 95.6°).

Particle Sizes of Na^+-Mnt and OMnt in Water

For Na^+-Mnt, the cumulative volume of the particle size <5 μm accounted for 99.7% in deionized water (Table 3). The result was in accord with the sizes of Na^+-Mnt particles ($\sim\leq 4$ μm) estimated according to Stokes' law in the purification by particle sedimentation.

100% of the OMnt particles were kept as <10 μm in deionized water (Fig. 7). The D_{50} values of the OMnt particles were 0.7–1.0 μm, similar to that of Na^+-Mnt (0.9 μm). The D_{99} value of CO/Mnt (7.6 μm) was greater than that of Na^+-Mnt (3.9 μm) (Table 3). These results indicated that the CO/Mnt particles were increased in size over Na^+-Mnt due to the CTAB and OTAC modification. A similar phenomenon was observed by Moslemizadeh et al. (2016). Particle sizes and swelling in water depend on delamination of platelets or dissociation of particles by crystalline or osmotic swelling. Na^+-Mnt is hydrophilic and adsorbs water easily, which results in osmotic swelling. Such osmotic swelling led to Mnt platelet delamination or particle dissociation (Moslemizadeh et al., 2016). The degree of osmotic swelling of CO/Mnt was less than that for Na^+-Mnt because its hydrophilicity was less; full

https://doi.org/10.1007/s42860-021-00149-2 Published online by Cambridge University Press

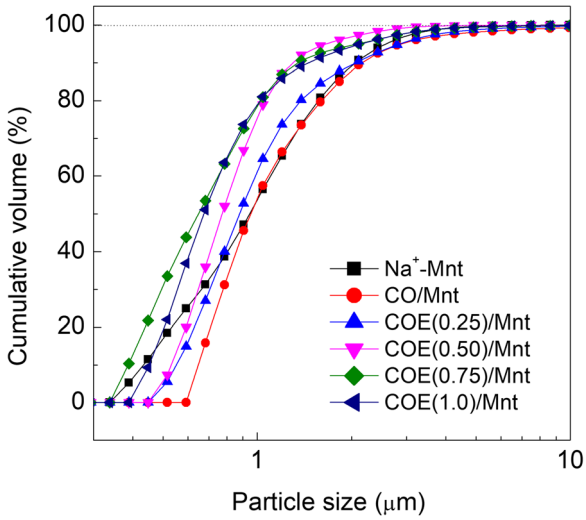

Fig. 7. Cumulative size distribution of the particles of Na^+-Mnt and OMnts

crystalline swelling for CO/Mnt was difficult because of an incomplete intercalation of CTA^+ and OTA^+ cations (<1 CEC) into the interlayer spaces of Mnt. As a result, the platelets of CO/Mnt hold together tightly in water.

The D_{99} value of E(1.5)/Mnt (4.9 μm) was also greater than that of Na^+-Mnt (3.9 μm), for two reasons: no crystalline swelling occurred because EA molecules were not intercalated into the interlayer spaces of Mnt; and, the EA molecules adsorbed on the external surfaces of Mnt prevented water from permeating into the pores of Mnt. The large surface hydrophobicity for E(1.5)/Mnt was not beneficial for osmotic swelling.

Most (99.4–99.9%) of the COE(x)/Mnt (x = 0.50−1.0) particles were retained as <5 μm in deionized water. Compared to CO/Mnt (7.6 μm), COE(x)/Mnt exhibited a smaller D_{99} value (2.7−5.4 μm) in deionized water due to crystalline swelling. The EA molecules adsorbed in the interlayer spaces

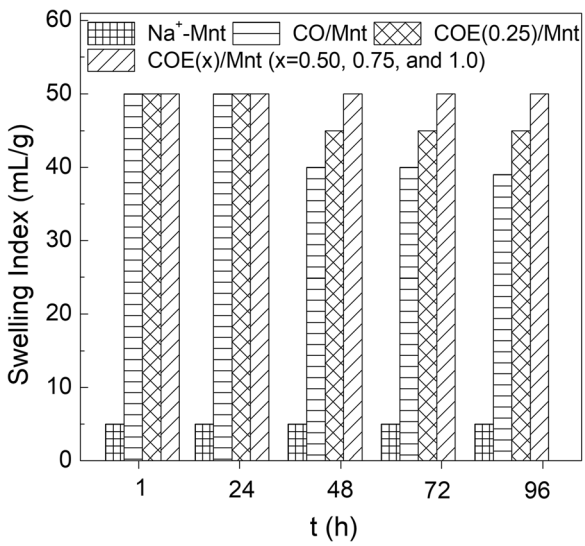

Fig. 8. Effect of time on the dispersion stability of the OMnt suspensions in xylene

of Mnt weakened the electrostatic forces between platelets of COE(x)/Mnt. Thus, the particles of COE(x)/Mnt were easier to dissociate than those of CO/Mnt.

Particle Sizes of OMnt in Xylene

The average particle sizes of COE(x)/Mnt (2.8–2.1 μm) in xylene were smaller than that of CO/Mnt (3.8 μm) in xylene. The particle sizes of COE(x)/Mnt decreased with an increase in the amount of EA added, from 0.25 CEC to 1.0 CEC in the OMnt preparation (Table 3). The particle sizes and the swelling in xylene depend on Mnt crystalline swelling and steric repulsion. Firstly, the XRD results above proved that COE(x)/Mnt had a greater level of intercalation and more ordered arrangements of the surfactants in the interlayer spaces of Mnt than CO/Mnt. Hence, COE(x)/Mnt was easier to exfoliate into single Mnt platelets or smaller particle sizes than CO/Mnt. Besides, the EA molecules adsorbed on Mnt could prevent the Mnt platelets from agglomeration due to steric hindrance. The EA molecule has a super-long carbon chain structure with a *cis* spatial conformation; this conformation prevented extensive associations among the OMnt particles. The steric repulsive forces among the particles improved the long-term dispersibility of OMnt in solvents (Zhang et al., 2013).

Swelling Indices of OMnt in Xylene

Swelling indices of OMnt in xylene (Fig. 8) reflect the dispersion degree of the OMnts. The swelling of Na^+-Mnt in xylene was small (5 mL/g after 1 h and stable thereafter) due to its high hydrophilicity. The swelling indices were 50 and 39 mL/g for CO/Mnt after static placement for up to 24 h and 48–96 h, respectively, whereas for COE(0.25)/Mnt, the swelling indices were 50 and 45 mL/g. Apparently, standing for 48 h or more enabled CO/Mnt and COE(0.25)/Mnt to reach a stable swelling state in xylene. The swelling indices of COE(x)/Mnt (x = 0.50, 0.75, and 1.0) reached a stable value of 50 mL/g during 1–96 h. The result indicated that COE(x)/Mnts were high swelling materials (Zhuang et al., 2015). Clearly, the swelling indices of COE(x)/Mnt were greater than that of CO/Mnt in xylene. Hence, co-modification of Mnt with ternary surfactants of CTAB, OTAC, and EA improved dramatically the dispersion stability of OMnt in xylene. The result was probably due to the following four reasons: (1) the average particle sizes of COE(x)/Mnt (2.8–2.1 μm) were smaller than that of CO/Mnt (3.8 μm) in xylene. The particles with small sizes prevented settling and were beneficial for high dispersibility of OMnt in solvents (Marras et al., 2007; Fan et al., 2015). (2) The large amount of adsorption of the CTAB, OTAC, and EA surfactants in the interlayer spaces of Mnt brought about exfoliation of more Mnt platelets. (3) The concentration of the EA molecules adsorbed on the surfaces of Mnt affected the stability of the COE(x)/Mnt particle suspensions in xylene. When the surfactant concentration of the OMnt suspensions in non-polar solvent reached a saturated state, the solid-liquid interfacial energy was a minimum and the dispersion was stable, according to Leach et al. (2005). (4) The super-long carbon chains with a *cis* spatial conformation of EA molecule increased the steric repulsive forces between

https://doi.org/10.1007/s42860-021-00149-2 Published online by Cambridge University Press

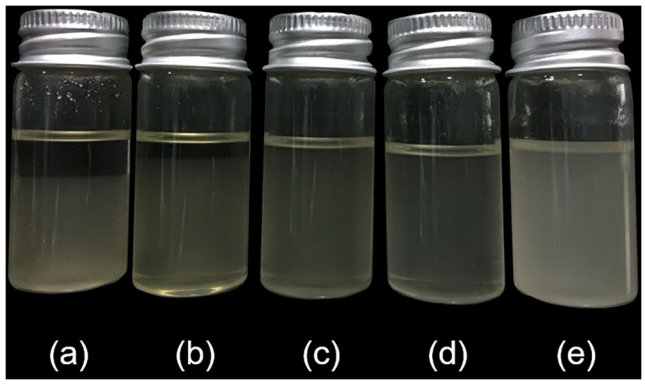

Fig. 9. Images of the 48 h settling of the suspensions of **a**CO/Mnt and **b** COE(*x*)/Mnt: *x* = 0.25, **c** 0.50, **d** 0.75, and **e** 1.0. Note: the concentration of OMnt in xylene was 0.02 g/mL

the particles. The steric stabilization of particles in xylene made the suspensions of COE(*x*)/Mnt more stable (Zhang et al., 2013).

The suspensions of CO/Mnt and COE(*x*)/Mnt (*x* = 0.25 and 1.0) in xylene looked turbid (Fig. 9) due to a low level of platelet exfoliation in xylene for CO/Mnt and COE(0.25)/Mnt or high surfactant coverage on the external surfaces of COE(1.0)/Mnt. The suspensions of COE(*x*)/Mnt (*x* = 0.50 and 0.75) were clearer than those of CO/Mnt and COE(*x*)/Mnt (*x* = 0.25 and 1.0).

Swelling Mechanisms of OMnt in Xylene

Mnt is composed of nanoplatelets (Ho & Glinka, 2003). The thickness of individual platelets was ~1 nm and they were ~0.5–1 μm long (Le Pluart et al., 2004). A few platelets were assembled to form the primary particles of Mnt (referred to as tactoids) by face-to-face association due to electrostatic attractions (Burgentzlé et al., 2004). The platelets of Mnt exposed two different surfaces (i.e. the crystal plane face and the crystal edge). On the crystal plane face surfaces of the platelets, negative charges exist. At the

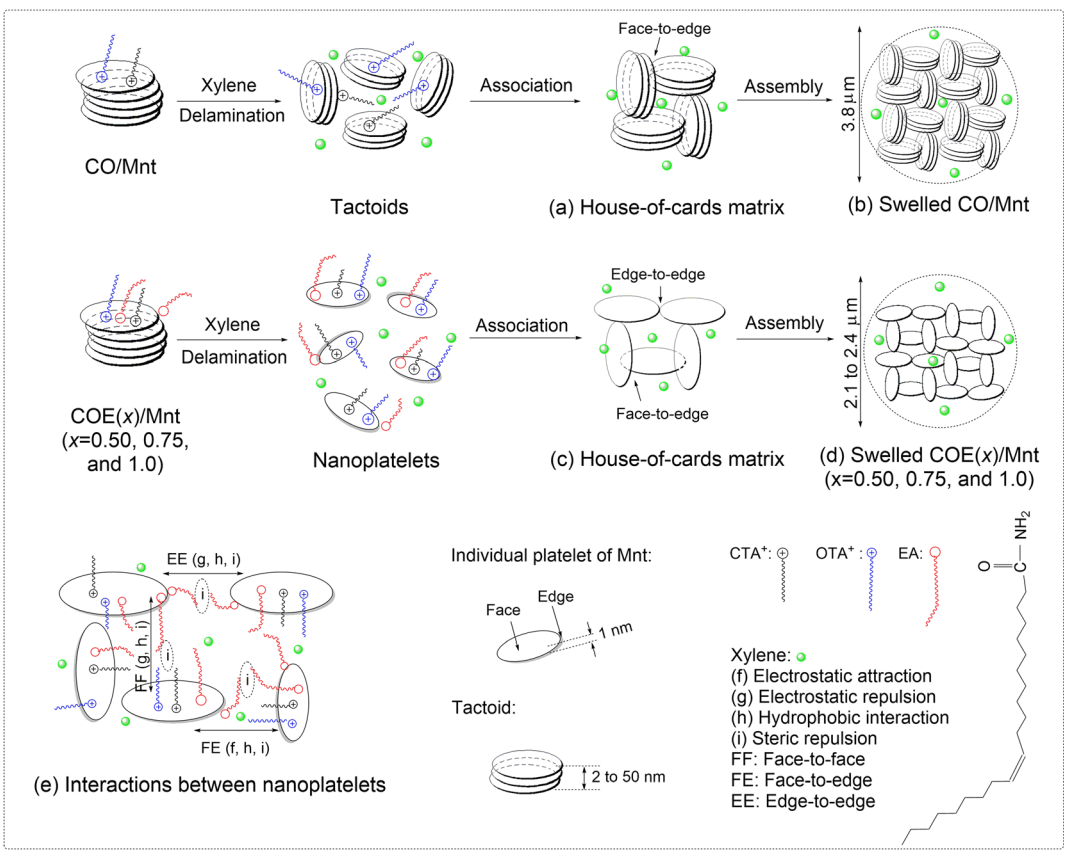

Fig. 10. Swelling mechanisms of OMnts in xylene

https://doi.org/10.1007/s42860-021-00149-2 Published online by Cambridge University Press

edge surfaces of platelets, the charge is positive under neutral and acidic conditions due to the disruption of Mnt lattice and the exposure of broken bonds (van Olphen, 1964).

Based on the particle sizes and the swelling states of CO/Mnt and COE(x)/Mnt in xylene, probable swelling mechanisms were proposed (Fig. 10). When CO/Mnt was dispersed in xylene, the platelets of CO/Mnt were partly delaminated to form tactoids and the tactoids were kept tightly packed due to the low level of intercalation of CTA^+ and OTA^+ into the interlayer spaces of Mnt. The tactoids were associated with the large particles (house-of-cards matrix, Fig. 10a) by face (negative)-to-edge (positive) association due to electrostatic attractions under the neutral environment (van Olphen, 1964; Burgentzlé et al., 2004). These house-of-cards matrices were assembled further to form larger particles, thus creating a large number of tactoids having a house-of-cards structure (Fig. 10b). While COE(x)/Mnt (x = 0.50, 0.75, and 1.0) was dispersed in xylene, the platelets were fully exfoliated to individual nanoplatelets because of high levels of intercalation of the surfactants into the interlayer spaces of Mnt. The strong electrostatic repulsion between the negatively charged nanoplatelets (face-to-face repulsion) kept the individual nanoplatelets separate. Similarly, the negative faces were attracted by the positive edges of the nanoplatelets (face-to-edge attraction) (Lagaly, 1981; Patel et al., 2007). Moreover, the hydrophobic groups of the EA molecules adsorbed at the edges of the Mnt nanoplatelets were drawn to each other by hydrophobic interactions (edge-to-edge). Thus, the single Mnt nanoplatelets were associated to form the house-of-cards matrix (Fig. 10c). These house-of-cards matrices were also associated further with larger house-of-cards matrices throughout the suspension (Fig. 10d). The super-long carbon chain structure with the *cis* spatial conformation of EA molecules led to steric repulsions between the Mnt nanoplatelets. Face-to-edge attraction, face-to-face repulsion, edge-to-edge repulsion, and the face-to-face, face-to-edge, and edge-to-edge hydrophobic interactions and steric repulsions led to more stable dispersion and smaller particle sizes of COE(x)/Mnt (x = 0.50, 0.75, and 1.0) (Fig. 10e) than those of CO/Mnt in xylene.

CONCLUSIONS

Hydrophobic OMnts with large surface area were successfully prepared by the co-modification of Na^+-Mnt with ternary surfactants CTA^+, OTA^+, and EA. Such co-modification achieved three improvements: (1) the surface hydrophobicity of OMnt increased and a maximum contact angle (95.6°) was obtained for COE (0.75)/Mnt; (2) high swellability and dispersion stability with a 50 mL/g of swelling index in xylene were obtained; and (3) the OMnt particles in xylene and water were refined.

In addition to the swelling, the nanoplatelets or the tactoids of OMnt in xylene were delaminated further and then assembled to a house-of-cards structure by face-to-edge and edge-to-edge configurations. This gave the OMnt high swellability and high dispersion stability. The process and structure involved electrostatic attractions, electrostatic and steric repulsions, and hydrophobic interactions.

ACKNOWLEDGMENTS

This work was supported by the National Natural Science Foundation of China [22072136, 21506188, 41672033]; Engineering Research Center of Non-metallic Minerals of Zhejiang Province, Zhejiang Institute of Geology and Mineral Resource, Hangzhou, China [ZD2020K07]; and the Zhejiang Provincial Natural Science Foundation of China [LY16B030010, LQ19F050004]. This work is also dedicated to the 5th anniversary (2017-2021) of the foundation of Qing Yang Institute for Industrial Minerals (QYIM, www.qyim-cn.com).

FUNDING

Funding sources are as stated in the Acknowledgments.

Declarations

Conflict of Interest

The authors declare that they have no conflict of interest.

REFERENCES

Alghunaim, A., Kirdponpattara, S., & Newby, B. M. Z. (2016). Techniques for determining contact angle and wettability of powders. *Powder Technology, 287*, 201–215.

Burgentzlé, D., Duchet, J., Gerard, J. F., Jupin, A., & Fillon, B. (2004). Solvent-based nanocomposite coatings I. Dispersion of organophilic montmorillonite in organic solvents. *Journal of Colloid and Interface Science, 278*(*1*), 26–39.

de Jong, S. M., Spiers, C. J., & Busch, A. (2014). Development of swelling strain in smectite clays through exposure to carbon dioxide. *International Journal of Greenhouse Gas Control, 24*, 149–161.

Fan, J. T., Zhu, H., Li, R., & Chen, N. J. (2015). Montmorillonite modified by cationic and nonionic surfactants as high-performancefluid-loss-control additive in oil-based drilling fluids. *Journal of Dispersion Science and Technology, 36*(*4*), 569–576.

Ghazy, O. A., Khalil, S. A., & Senna, M. M. (2020). Synthesis of montmorillonite/chitosan/ammonium acrylate composite and its potential application in river water flocculation. *International Journal of Biological Macromolecules, 163*, 1529–1537.

Hamberger, A., & Stenhagen, G. (2003). Erucamide as a modulator of water balance: new function of a fatty acid amide. *Neurochemical Research, 28*(*2*), 177–185.

He, H. P., Ma, Y. H., Zhu, J. X., Yuan, P., & Qing, Y. H. (2010). Organoclays prepared from montmorillonites with different cation exchange capacity and surfactant configuration. *Applied Clay Science, 48(1–2)*, 67–72.

Ho, D. L., & Glinka, C. J. (2003). Effects of solvent solubility parameters on organoclay dispersions. *Chemistry of Materials, 15*(*6*), 1309–1312.

Ikhtiyarova, G. A., Özcan, A. S., Gök, Ö., & Özcan, A. (2012). Characterization of natural- and organo-bentonite by XRD, SEM, FT-IR and thermal analysis techniques and its adsorption behaviour in aqueous solutions. *Clay Minerals, 47*(*1*), 31–44.

Khenifi, A., Bouberka, Z., Sekrane, F., Kameche, M., & Derriche, Z. (2007). Adsorption study of an industrial dye by an organic clay. *Adsorption – Journal of the International Adsorption Society, 13*(*2*), 149–158.

Kooli, F., Liu, Y., Alshahateet, S. F., Messali, M., & Bergaya, F. (2009). Reaction of acid activated montmorillonites with hexadecyl trimethylammonium bromide solution. *Applied Clay Science, 43(3–4)*, 357–363.

Lagaly, G. (1981). Characterization of clays by organic compounds. *Clay Minerals, 16*, 1–21.

https://doi.org/10.1007/s42860-021-00149-2 Published online by Cambridge University Press

Lapides, I., Borisover, M., & Yariv, S. (2011). Thermal analyis of hexadecyltrimethylammonium-montmorillonites. *Journal of Thermal Analysis and Calorimetry, 105*(*3*), 921–929.

Le Pluart, L., Duchet, J., Sautereau, H., Halley, P., & Gerard, J. F. (2004). Rheological properties of organoclay suspensions in epoxy network precursors. *Applied Clay Science, 25(3–4)*, 207–219.

Leach, E. S. H., Hopkinson, A., Franklin, K., & Van Duijneveldt, J. S. (2005). Nonaqueous suspensions of laponite and montmorillonite. *Langmuir, 21*(*9*), 3821–3830.

Li, Y. Q., & Ishida, H. (2003). Concentration-dependent conformation of alkyl tail in the nanoconfined space: Hexadecylamine in the silicate galleries. *Langmuir, 19*(*6*), 2479–2484.

Liao, L. B., Lv, G. C., Cai, D. X., & Wu, L. M. (2016). The sequential intercalation of three types of surfactants into sodium montmorillonite. *Applied Clay Science, 119*, 82–86.

Madejová, J. (2003). FTIR techniques in clay mineral studies. *Vibrational Spectroscopy, 31*(*1*), 1–10.

Madejová, J., & Komadel, P. (2001). Baseline studies of The Clay Minerals Society source clays: infrared methods. *Clays and Clay Minerals, 49*(*5*), 410–432.

Marras, S. I., Tsimpliaraki, A., Zuburtikudis, I., & Panayiotou, C. (2007). Thermal and colloidal behavior of amine-treated clays: The role of amphiphilic organic cation concentration. *Journal of Colloid and Interface Science, 315*(*2*), 520–527.

Meleshyn, A., & Bunnenberg, C. (2006). Interlayer expansion and mechanisms of anion sorption of Na-montmorillonite modified by cetylpyridinium chloride: A Monte Carlo study. *The Journal of Physical Chemistry B, 110*, 2271–2277.

Monteiro, M. K. S., de Oliveira, V. R. L., dos Santos, F. K. G., Neto, E. L. D., Leite, R. H. D., Aroucha, E. M. M., & Silva, K. N. D. (2018). Influence of the ionic and nonionic surfactants mixture in the structure and properties of the modified bentonite clay. *Journal of Molecular Liquids, 272*, 990–998.

Moraru, V. N. (2001). Structure formation of alkylammonium montmorillonites in organic media. *Applied Clay Science, 19(1–6)*, 11–26.

Moreira, J. F. M., Alves, T. S., Barbosa, R., de Carvalho, E. M., & Carvalho, L. H. (2016). Effect of cis-13-docosenamide in the properties of compatibilized polypropylene/clay nanocomposites. *Macromolecular Symposia, 367*(*1*), 68–75.

Moslemizadeh, A., Aghdam, S. K. Y., Shahbazi, K., Aghdam, H. K. Y., & Alboghobeish, F. (2016). Assessment of swelling inhibitive effect of CTAB adsorption on montmorillonite in aqueous phase. *Applied Clay Science, 127*, 111–122.

Parolo, M. E., Pettinari, G. R., Musso, T. B., Sanchez-Izquierdo, M. P., & Fernandez, M. L. G. (2014). Characterization of organo-modified bentonite sorbents: The effect of modification conditions on adsorption performance. *Applied Surface Science, 320*, 356–363.

Patel, H. A., Somani, R. S., Bajaj, H. C., & Jasra, R. V. (2007). Preparation and characterization of phosphonium montmorillonite with enhanced thermal stability. *Applied Clay Science, 35(3–4)*, 194–200.

Poisson, C., Hervais, V., Lacrampe, M. F., Krawczak, P., Falher, T., Gondard, C., & Ferreiro, V. (2010). Optimization of polyethylene/binder/polyamide extrusion blow-molded films. iii. slippability improvement with fatty acid amides. *Journal of Applied Polymer Science, 115*(*4*), 2332–2345.

Ratnayake, U. N., Haworth, B., & Hourston, D. J. (2009). Preparation of polypropylene-clay nanocomposites by the co-intercalation of modified polypropylene and short-chain amide molecules. *Journal of Applied Polymer Science, 112*(*1*), 320–334.

Salles, F., Bildstein, O., Douillard, J. M., Jullien, M., & Van Damme, H. (2007). Determination of the driving force for the hydration of the swelling clays from computation of the hydration energy of the interlayer cations and the clay layer. *Journal of Physical Chemistry C, 111*(*35*), 13170–13176.

Sankhe, S. Y., & Hirt, D. E. (2002). Characterization of erucamide profiles in multilayer linear low-density polyethylene and propylene-ethylene copolymer films using synchrotron-based FT-IR microspectroscopy. *Applied Spectroscopy, 56*(*2*), 205–211.

Sankhe, S. Y., Janorkar, A. V., & Hirt, D. E. (2003). Characterization of erucamide profiles in LLDPE films: depth-profiling attempts using FTIR photoacoustic spectroscopy and Raman microspectroscopy. *Journal of Plastic Film & Sheeting, 19(1)*, 16–29.

Shah, K. J., Mishra, M. K., Shukla, A. D., Imae, T., & Shah, D. O. (2013). Controlling wettability and hydrophobicity of organoclays modified with quaternary ammonium surfactants. *Journal of Colloid and Interface Science, 407*, 493–499.

Shattar, S. F. A., Zakaria, N. A., & Foo, K. Y. (2020). One step acid activation of bentonite derived adsorbent for the effective remediation of the new generation of industrial pesticides. *Scientific Reports, 10*, 20151.

Shuler, C. A., Janorkar, A. V., & Hirt, D. E. (2004). Fate of erucamide in polyolefin films at elevated temperature. *Polymer Engineering and Science, 44*(*12*), 2247–2253.

Teich-McGoldrick, S. L., Greathouse, J. A., Jove-Colon, C. F., & Cygan, R. T. (2015). Swelling properties of montmorillonite and beidellite clay minerals from molecular simulation: comparison of temperature, interlayer cation, and charge location effects. *Journal of Physical Chemistry C., 119*(*36*), 20880–20891.

van Olphen, H. (1964). Internal mutual flocculation in clay suspensions. *Journal of Colloid Science, 19*(*4*), 313–322.

Veiskarami, M., Sarvi, M. N., & Mokhtari, A. R. (2016). Influence of the purity of montmorillonite on its surface modification with an alkyl-ammonium salt. *Applied Clay Science, 120*, 111–120.

Xi, Y. F., Ding, Z., He, H. P., & Frost, R. L. (2004). Structure of organo-clays– an X-ray diffraction and thermogravimetric analysis study. *Journal of Colloid and Interface Science, 277*(*1*), 116–120.

Xi, Y. F., Frost, R. L., He, H. P., Kloprogge, T., & Bostrom, T. (2005). Modification of Wyoming montmorillonite surfaces using a cationic surfactant. *Langmuir, 21*(*19*), 8675–8680.

Xi, Y. F., Zhou, Q., Frost, R. L., & He, H. P. (2007). Thermal stability of octadecyltrimethylammonium bromide modified montmorillonite organoclay. *Journal of Colloid and Interface Science, 311*(*2*), 347–353.

Yu, W. H., Ren, Q. Q., Tong, D. S., Zhou, C. H., & Wang, H. (2014). Clean production of CTAB-montmorillonite: formation mechanism and swelling behavior in xylene. *Applied Clay Science, 97*, 222–234.

Yu, W. H., Zhu, T. T., Tong, D. S., Wang, M., Wu, Q. Q., & Zhou, C. H. (2017). Preparation of organo-montmorillonites and the relationship between microstructure and swellability. *Clays and Clay Minerals, 65*(*6*), 417–430.

Zatta, L., Ramos, L. P., & Wypych, F. (2013). Acid-activated montmorillonites as heterogeneous catalysts for the esterification of lauric acid acid with methanol. *Applied Clay Science. 80–81*, 236–244.

Zhang, M., Li, L., Xu, J., & Sun, D. J. (2013). Effect of polyisobutylenesuccinimide on low-temperature rheology and dispersibility of clay particles in mineral oil. *Colloids and Surfaces A – Physicochemical and Engineering Aspects, 431*, 133–141.

Zhou, C. H., Li, C. J., Gates, W. P., Zhu, T. T., & Yu, W. H. (2019). Co-intercalation of organic cations/amide molecules into montmorillonite with tunable hydrophobicity and swellability. *Applied Clay Science, 179*, 105157.

Zhu, R. L., Zhu, L. H., Zhu, J. X., & Xu, L. H. (2008). Structure of cetyltrimethylammonium intercalated hydrobiotite. *Applied Clay Science, 42(1–2)*, 224–231.

Zhuang, G. Z., Zhang, Z. P., Fu, M., Ye, X., & Liao, L. B. (2015). Comparative study on the use of cationic-nonionic-organo-montmorillonite in oil-based drilling fluids. *Applied Clay Science, 116*, 257–262.

Zhuang, G. Z., Zhang, Z. P., Sun, J. L., & Liao, L. B. (2016). The structure and rheology of organo-montmorillonite in oil-based system aged under different temperatures. *Applied Clay Science, 124*, 21–30.

(Received 12 May 2021; revised 29 July 2021; AE: Jun Kawamata)